F-electron spectral function of the Falicov-Kimball model in infinite dimensions: The half-filled case

J. K. Freericks* and V. M. Turkowski†
Department of Physics, Georgetown University, Washington, DC 20057, USA

V. Zlatić‡
Institute of Physics, Bijenicka c. 46, P.O.B. 304, 10000 Zagreb, Croatia
(Received 15 July 2004; revised manuscript received 3 November 2004; published 17 March 2005)

The *f*-electron spectral function of the Falicov-Kimball model is calculated via a Keldysh-based many-body formalism originally developed by Brandt and Urbanek. We provide results for both the Bethe lattice and the hypercubic lattice at half filling. Since the numerical computations are quite sensitive to the discretization along the Kadanoff-Baym contour and to the maximum cutoff in time that is employed, we analyze the accuracy of the results using a variety of different moment sum rules and spectral formulas. We find that the *f*-electron spectral function has interesting temperature dependence, becoming a narrow single-peaked function for small *U* and developing a gap, with two broader peaks for large *U*.

DOI: 10.1103/PhysRevB.71.115111 PACS number(s): 71.10.−w, 71.27.+a, 71.30.+h

I. INTRODUCTION

Nonequilibrium many-body physics is becoming an increasingly important field because it allows strongly correlated electrons to be examined in the presence of large external fields, which can drive them far from equilibrium; as nanotechnology research grows, there are an increasing number of nanoscale solid-state devices which are exposed to extreme fields. The formalism to solve nonequilibrium problems was developed independently by Kadanoff and Baym[1] and by Keldysh.[2] In principle, it allows these nonequilibrium problems to be solved exactly (including all nonlinear field effects), but usually the formalism is employed in a perturbative approach for the electron correlations. These nonequilibrium formalisms can also be used to calculate equilibrium Green's functions, especially in cases where alternative analytic continuation methods are intractable. We examine the simplest such problem—the *f*-electron spectrum of the Falicov-Kimball model. This problem can be solved exactly with dynamical mean-field theory (DMFT).

The spinless Falicov-Kimball model[3] (FK) describes the dynamics of two types of electrons: conduction electrons (created or destroyed at site i by $d^\dagger$ or d) and localized electrons (created or destroyed at site i by $f^\dagger$ or f). The noninteracting conduction electrons can hop between nearest-neighbor sites on a D-dimensional lattice, with a hopping matrix $-t_{ij}=-t^*/2\sqrt{D}$; we choose a scaling of the hopping matrix that yields a nontrivial limit in infinite dimensions.[4] The f electrons have a site energy E_f, and a chemical potential μ is employed to adjust the total number of electrons $n_d+n_f=n_{tot}$. The d- and f-number operators at each site are n_d and n_f. There is a finite Coulomb interaction U between d- and f electrons that occupy the same lattice site, and so the Falicov-Kimball Hamiltonian for the lattice is

$$\mathcal{H}_{FK}=\sum_{ij}(-t_{ij}-\mu\delta_{ij})d_i^\dagger d_j+\sum_i(E_f-\mu)f_i^\dagger f_i+\sum_i U d_i^\dagger d_i f_i^\dagger f_i. \tag{1}$$

The FK lattice model [in Eq. (1)] can be solved in infinite dimensions using the methods of Brandt and Mielsch.[5] We consider two kinds of lattices: (i) the hypercubic lattice with a Gaussian noninteracting density of states $\rho_{hc}(\epsilon)=\exp[-\epsilon^2/t^{*2}]/(\sqrt{\pi}t^*)$, and (ii) the infinite-coordination Bethe lattice with a semicircular noninteracting density of states $\rho_B(\epsilon)=\sqrt{4t^{*2}-\epsilon^2}/(2\pi t^{*2})$; we take t^* as the unit of energy ($t^*=1$), and consider only the homogeneous phase, where all quantities are translationally invariant. For our numerical work, we will concentrate on half filling, where $\mu=U/2$ and $E_f=0$.

Despite the conservation of the local f-electron number ($[\mathcal{H}_{FK},f_i^\dagger f_i]=0$), the f electrons have nontrivial dynamics as a function of T,[6,7] so we expect the f-electron spectral function to have an interesting evolution with the correlation strength U. When $U=0$, the spectral function is a delta function, which broadens as U increases because the f electron sees a fluctuating d electron that hops onto and off of the local site as a function of time. When U is increased further, a metal-insulator transition takes place, and we expect the f-spectral function to develop a gap as $T\to 0$. Hence, the f-electron spectral function should have rich behavior as a function of U and T.

The organization of this paper is as follows. In Sec. II, we present the formalism, outlining in detail how the analytic continuation is carried out within this nonequilibrium approach; our notation is nonstandard because we use the usual Kadanoff-Baym contour, but we stick with the Green's function definitions for $G^>$ and $G^<$ of Brandt and Urbanek.[8] In Sec. III, we present our numerical results for both the Bethe

and hypercubic lattices, and we conclude in Sec. IV. A short communication, showing the spectral function at the critical or near-critical value of U for the metal-insulator transition, has been completed,[9] and a longer contribution, detailing the computational algorithm, parallelization, and numerical accuracy, has also been completed.[10]

II. FORMALISM

The many-body problem on an infinite-coordination lattice can be solved by a mean-field-like procedure, because the self-energy of the conduction electrons is local.[4] Hence, the local d-electron Green's function $G_{loc}(z)$ on the lattice satisfies

$$G_d^{loc}(z) = \int \frac{\rho(\epsilon)}{z + \mu - \Sigma_d(z) - \epsilon} d\epsilon, \tag{2}$$

where z is a complex variable and Σ_d is the momentum-independent self-energy. As noted by Brandt and Mielsch,[5] the lattice self-energy coincides with the self-energy of an atomic d state coupled to an f state with the same Coulomb interaction as on the lattice, and perturbed by an external time-dependent field, $\lambda(\tau,\tau')$, which mimics, for the impurity, the hopping of the conduction electrons on the lattice, by creating time-dependent fluctations of the conduction-electron density. For an appropriate choice of the λ field, the functional dependence of Σ_d on $G_d(z)$ and $G_f(z)$, the atomic propagators for d- and f states, is exactly the same as in the lattice case. The lattice problem is thus reduced to finding the atomic self-energy functional for the d electrons, and then setting $G_d^{loc}(z)=G_d(z)$ and $G_f^{loc}(z)=G_f(z)$ on each lattice site.

The FK atom can be solved by using the interaction representation, such that the time dependence of operators is defined by the atomic Hamiltonian

$$\mathcal{H}_{at} = -\mu d^\dagger d + (E_f - \mu) f^\dagger f + U d^\dagger d f^\dagger f, \tag{3}$$

and the time dependence of the state vectors is governed by an evolution operator which is defined by the λ field. For purely imaginary times, $\overline{\tau} \in (0, -i\beta)$, the evolution operator is

$$S(\overline{\tau},\lambda) = T_{\overline{\tau}} e^{+\int_0^{\overline{\tau}} d\overline{\tau}' \int_0^{\overline{\tau}} d\overline{\tau}'' \lambda(\overline{\tau}',\overline{\tau}'') d^\dagger(\overline{\tau}') d(\overline{\tau}'')}, \tag{4}$$

where $T_{\overline{\tau}}[\cdots]$ orders all the operators within the bracket with respect to the position on the line $(0,-i\beta)$ of their time argument in such a way that the time arguments which are closer to zero appear further to the right, and there is an overall change of sign whenever the time ordering interchanges two fermionic operators. The time evolution of the operators between an initial time $\overline{\tau}'$ and the final time $\overline{\tau}$ is determined by $\mathcal{H}_{at}$ as

$$O(\overline{\tau}) = e^{i(\overline{\tau}-\overline{\tau}')\mathcal{H}_{at}} O(\overline{\tau}') e^{-i(\overline{\tau}-\overline{\tau}')\mathcal{H}_{at}}. \tag{5}$$

The integration is along the imaginary-time axis ($\overline{\tau}$ and $\overline{\tau}'$ are purely imaginary), i.e., our time variable $\overline{\tau}$ can be expressed in terms of Brandt and Mielsch's[5] variable τ in the following way: $\overline{\tau}=-i\tau$.

The atomic Hamiltonian $\mathcal{H}_{at}$ and the time-dependent field $\lambda(\overline{\tau},\overline{\tau}')$ define the partition function of the FK atom

$$\mathcal{Z}_{at}(\lambda,\mu,\beta) = \mathrm{Tr}_{df}\, T_{\overline{\tau}}[\exp\{-\beta\mathcal{H}_{at}\} S(-i\beta,\lambda)], \tag{6}$$

where the trace is taken over the atomic d- and f states. Since the number of f electrons is a conserved quantity, we can write

$$\mathcal{Z}_{at}(\lambda) = \mathcal{Z}_0(\lambda,\mu) + e^{-\beta(E_f-\mu)} \mathcal{Z}_0(\lambda,\mu-U), \tag{7}$$

with $Z_0(\lambda,\mu)$ the partition function of a d electron subject to the λ field in the absence of f electrons ($n_f=0$). That is, $Z_0(\lambda,\mu)=\mathrm{Tr}_d\, T_{\overline{\tau}}[\exp\{-\beta\mathcal{H}_0\} S(-i\beta,\lambda)]$, where $\mathcal{H}_0=-\mu d^\dagger d$.

The field $\lambda(\overline{\tau},\overline{\tau}')$ gives rise to fluctuations in the d occupancy, which correspond in the equivalent lattice problem to the local d fluctuations due to the d-electron hopping. We choose $\lambda(\overline{\tau},\overline{\tau}')$ such that it satisfies the same (antiperiodic) boundary condition as the imaginary-time Green's function (see below), and expand it in a Fourier series along the imaginary axis (recall $\overline{\tau}$ is purely imaginary)

$$\lambda(\overline{\tau}-\overline{\tau}') = T\sum_n e^{\omega_n(\overline{\tau}-\overline{\tau}')} \lambda_n. \tag{8}$$

Here, $\omega_n=\pi(2n+1)T$ is the fermionic Matsubara frequency and we set $k_B=1$. The λ field in the complex ω plane, which is needed for the f-electron propagator, can be determined by an iterative procedure using the DMFT self-consistency condition for the d-electron's Green's function.

The d-electron Green's function is defined as a functional derivative of the atomic partition function,[1] $G_d(\overline{\tau}-\overline{\tau}') = \delta \ln \mathcal{Z}_{at}/\delta\lambda(\overline{\tau}',\overline{\tau})$, which gives

$$G_d(\overline{\tau}-\overline{\tau}') = -\frac{1}{\mathcal{Z}_{at}} \mathrm{Tr}_{df}\, T_{\overline{\tau}}[e^{-\beta\mathcal{H}_{at}} S(-i\beta,\lambda) d(\overline{\tau}) d^\dagger(\overline{\tau}')]. \tag{9}$$

$G_f(\overline{\tau}-\overline{\tau}')$ is periodic on the imaginary time axis with period $2i\beta$, and is antiperiodic modulo$(i\beta)$. It depends on the difference of the time arguments, because we are in thermal equilibrium and the system is time-translation invariant; it has a discontinuity at $\overline{\tau}=\overline{\tau}'$ and is therefore a nonanalytic function of $\overline{\tau}-\overline{\tau}'$.

To find G_f we define the effective-medium Green's function, $G_d^0(\overline{\tau}-\overline{\tau}') = \delta \ln \mathcal{Z}_0/\delta\lambda(\overline{\tau}',\overline{\tau})$, which reads

$$G_d^0(\overline{\tau}-\overline{\tau}') = -\frac{1}{\mathcal{Z}_0(\lambda,\mu)} \mathrm{Tr}_d\, T_{\overline{\tau}}[e^{-\beta\mathcal{H}_0} S(-i\beta,\lambda) d(\overline{\tau}) d^\dagger(\overline{\tau}')], \tag{10}$$

and satisfies the equation of motion [EOM] (Ref. 1)

$$\int d\overline{\tau}''[(-\partial_{\overline{\tau}} + i\mu)\delta_c(\overline{\tau}-\overline{\tau}'') + \lambda(\overline{\tau}-\overline{\tau}'')] G_d^0(\overline{\tau}''-\overline{\tau}') = \delta_c(\overline{\tau}-\overline{\tau}'), \tag{11}$$

with $\delta_c(\overline{\tau})$ the delta function defined on the line segment $(0,-i\beta)$ with the normalization $\int d\overline{\tau}\delta_c(\overline{\tau})=1$ [i.e., $\delta_c(\overline{\tau}) = iT\Sigma_n \exp[\omega_n\overline{\tau}]$]. Since G_d^0 also satisfies the usual periodic boundary conditions, Fourier transforming the EOM gives the solution

$$[G_d^0(i\omega_n)]^{-1} = i\omega_n + \mu - \lambda_n, \tag{12}$$

and the full Green's function follows as[5,7]

$$G_d(i\omega_n) = \frac{w_0}{[G_d^0(i\omega_n)]^{-1}} + \frac{w_1}{[G_d^0(i\omega_n)]^{-1} - U}, \tag{13}$$

with w_0 and w_1 the statistical weighting factors of the unoccupied and the occupied f states, respectively. These are given by[5] $w_1 = 1 - w_0$ and $w_0 = \mathcal{Z}_0/\mathcal{Z}_{at}$, where

$$\mathcal{Z}_0(\lambda,\mu) = 2e^{\beta\mu/2}\prod_n \frac{[G_d^0(i\omega_n)]^{-1}}{i\omega_n}. \tag{14}$$

Defining the self-energy function of the FK atom Σ_d by Dyson's equation

$$\Sigma_d = [G_d^0]^{-1} - [G_d]^{-1}, \tag{15}$$

which holds on the imaginary and the real frequency axes, we can find the λ field and the statistical weighting factors w_0 and w_1 by an iterative procedure. We start with a trial self-energy on the imaginary axis and calculate G_d from Eq. (2), get $[G_d^0]^{-1}$ from Eq. (15), calculate w_0 and w_1 using Eqs. (14) and (7), recalculate G_d from (13), and find the new Σ_d from Eq. (15). Once the procedure is converged on the imaginary axis, we have the weights w_0 and w_1, the chemical potential μ, and the self-consistent solution for the λ field. Since w_0 and w_1 are just numbers, we can analytically continue $G_d(i\omega_n)$ given by Eq. (13) from the imaginary axis in the complex frequency plane and repeat the iterative procedure to find retarded quantities and the spectral function of the λ field. The knowledge of the λ field everywhere in the complex ω plane is a necessary input to find the Green's function of the localized f electrons.

The imaginary time Green's function of the f electrons is defined by an expression analogous to Eq. (9)

$$G_f(\overline{\tau} - \overline{\tau'}) = -\frac{1}{\mathcal{Z}_{at}}\mathrm{Tr}_{df}\, T_{\overline{\tau}}[e^{-\beta\mathcal{H}_{at}} S(-i\beta,\lambda) f(\overline{\tau}) f^{\dagger}(\overline{\tau'})]; \tag{16}$$

it satisfies the same boundary condition, and has the same analytic structure as $G_d(\overline{\tau} - \overline{\tau'})$. As usual, we express $G_f(\overline{\tau} - \overline{\tau'})$ in terms of two analytic functions of $\overline{\tau} - \overline{\tau'}$, such that

$$G_f(\overline{\tau} - \overline{\tau'}) = \begin{cases} G_f^{>}(\overline{\tau} - \overline{\tau'}) & \text{for } \mathrm{Im}(\overline{\tau} - \overline{\tau'}) < 0 \\ G_f^{<}(\overline{\tau} - \overline{\tau'}) & \text{for } \mathrm{Im}(\overline{\tau} - \overline{\tau'}) > 0 \end{cases}. \tag{17}$$

To find $G_f^{>}$ and $G_f^{<}$ we introduce the real variables $\tau = i\overline{\tau}$ and $\tau' = i\overline{\tau'}$, and represent $G_f(\overline{\tau} - \overline{\tau'})$ by the Matsubara sum

$$G_f(\overline{\tau} - \overline{\tau'}) = T\sum_n e^{-i\omega_n(\tau - \tau')} G_f(i\omega_n). \tag{18}$$

For $\tau - \tau' \in (-\beta, 0)$, which corresponds to $\mathrm{Im}(\overline{\tau} - \overline{\tau'}) \in (0, \beta)$, we replace the sum over Matsubara frequencies by a contour integral in the complex frequency plane. Using $\mathrm{Res} f(z)|_{iw_n} = -1/\beta$, where $f(\omega)$ is the Fermi function, we obtain

$$G_f^{<}(\overline{\tau} - \overline{\tau'}) = \int_{-\infty}^{\infty} d\omega\, f(\omega) e^{-\omega(\tau - \tau')} A_f(\omega), \tag{19}$$

where $A_f(\omega) = -\mathrm{Im}\, G_f^R(\omega)/\pi$ is the spectral function. Here, we used the fact that $G_f(z)$ coincides with the retarded Green's function, $G_f^R(z)$, in the upper half-plane and with the advanced Green's function, $G_f^A(z)$, in the lower half-plane, and that the discontinuity of $G_f(z)$ across the cut along the real ω axis is given by $[G_f^R(\omega + i0^+) - G_f^A(\omega - i0^+)]/2\pi i = -\mathrm{Im}\, G_f^R(\omega)/\pi$. Since $\tau - \tau' \in (-\beta, 0)$, the integrand is well behaved for $\omega \to \pm\infty$ (the cutoff at $\omega \to \infty$ is provided by the Fermi function) and the integral defines an analytic function (it has derivatives to all orders). Reinstating the imaginary times $\overline{\tau}$ and $\overline{\tau'}$, we obtain

$$G_f^{<}(\overline{\tau} - \overline{\tau'}) = \int_{-\infty}^{\infty} d\omega\, A_f(\omega) f(\omega) e^{-i\omega(\overline{\tau} - \overline{\tau'})}, \tag{20}$$

which can be used to perform the analytic continuation from the imaginary to real times, $\overline{\tau} \to t$, $\overline{\tau'} \to t'$. Defining the Fourier transform of the real-time Green's function as

$$G_f^{<}(t - t') = \frac{1}{2\pi}\int_{-\infty}^{\infty} d\omega\, e^{-i\omega(t - t')} G_f^{<}(\omega), \tag{21}$$

it follows that

$$G_f^{<}(\omega) = 2\pi A_f(\omega) f(\omega); \tag{22}$$

hence, our definition for $G^{<}$ and $G^{>}$ is missing a factor of i from the standard definition, but agrees with that of Brandt and Urbanek.[8] Similarly, for $\tau - \tau' \in (0, \beta)$ and $\mathrm{Im}(\overline{\tau} - \overline{\tau'}) \in (-\beta, 0)$, we use $\mathrm{Res} f(-z)|_{iw_n} = 1/\beta$ and express the Matsubara sum for $G_f^{>}(\tau - \tau')$ as

$$G_f^{>}(\overline{\tau} - \overline{\tau'}) = -\int_{-\infty}^{\infty} d\omega\, A_f(\omega) f(-\omega) e^{-i\omega(\overline{\tau} - \overline{\tau'})}. \tag{23}$$

This integrand is also well behaved and shows that $G_f^{>}$ is an analytic function of imaginary times. The analytic continuation to the real axis, $\overline{\tau} \to t$, $\overline{\tau'} \to t'$, gives

$$G_f^{>}(t - t') = \int_{-\infty}^{\infty} d\omega\, A_f(\omega)[f(\omega) - 1] e^{-i\omega(t - t')}, \tag{24}$$

so that the Fourier transform of $G_f^{>}(t)$ reads

$$G_f^{>}(\omega) = 2\pi A_f(\omega)[f(\omega) - 1]. \tag{25}$$

At half-filling, where $A_f(\omega) = A_f(-\omega)$, we use $G_f^{>}(t - t') = [G_f^{>}(t' - t)]^*$ and obtain from the inverse of Eq. (24) the result

$$A_f(\omega) = -\frac{2}{\pi}\int_0^{\infty} dt \cos(\omega t)\, \mathrm{Re}\, G_f^{>}(t). \tag{26}$$

Thus, the time-ordered Green's function at real times can be written as

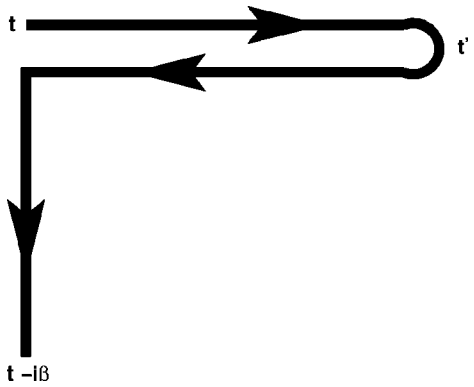

FIG. 1. Kadanoff-Baym contour for evaluating the equilibrium Green's function for $t \leq t'$. For $t \geq t'$ the contour starts at t' and runs to t, then goes back to t' and ends at $t' - i\beta$.

$$G_f(t-t') = \int d\omega\, A_f(\omega)[f(\omega) - \Theta(t-t')]e^{-i\omega(t-t')}, \quad (27)$$

with $\Theta(x)$ the unit step function $\Theta(x>0)=1$ and $\Theta(x<0)=0$.

However, these formal manipulations, which reveal the analytic properties of the Green's function, do not explicitly provide the spectral function, $A_f(\omega)$, which is needed to find $G_f^>$ or $G_f^<$. On the other hand, the imaginary-time formalism provides numerical results for the Green's function at the Matsubara frequencies[5,7,11] but it does not reveal the full analytic structure and it does not provide the spectral function. Thus, the real-time Green's function of the f electron cannot be inferred directly from these formal and numerical results but has to be calculated separately.

To obtain the real-time properties of the f electron, we define the contour-ordered Green's function in the interaction representation as

$$G_f^c(t-t') = -\frac{1}{\mathcal{Z}_{at}}\mathrm{Tr}_{df}\, T_c[e^{-\beta\mathcal{H}_{at}} S_c(\lambda_c) f(t) f^\dagger(t')], \quad (28)$$

where

$$S_c(\lambda_c) = T_c e^{\int_c d\bar{t}\int_c d\bar{t}'\lambda_c(\bar{t},\bar{t}')d^\dagger(\bar{t})d(\bar{t}')}, \quad (29)$$

is the analytic continuation of the evolution operator in Eq. (4) from imaginary times to times on the contour which is depicted in Fig. 1 for the case $t<t'$. For $t<t'$ the contour starts at t, runs to t', goes back to t, and ends at $t-i\beta$. Once again, this notation is missing a factor of i in the exponent of the evolution operator and as a prefactor for the Green's function, from that used in standard approaches, but it agrees with Brandt and Urbanek.[8]

The time dependence of the operators on the contour is defined as (assuming $\bar{t}'$ precedes $\bar{t}$ on C)

$$O(\bar{t}) = e^{i(\bar{t}-\bar{t}')\mathcal{H}_{at}} O(\bar{t}') e^{-i(\bar{t}-\bar{t}')\mathcal{H}_{at}}. \quad (30)$$

The $T_c[\cdots]$ orders all operators within the bracket with respect to the position on the contour of their time arguments, such that

$$T_c[f(\bar{t})f^\dagger(\bar{t}')] = \begin{cases} f(\bar{t})f^\dagger(\bar{t}') & \bar{t}' \text{ preceding } \bar{t} \text{ on } C \\ -f^\dagger(\bar{t}')f(\bar{t}) & \bar{t} \text{ preceding } \bar{t}' \text{ on } C \end{cases}, \quad (31)$$

and similarly for the d operators.

The λ field on the contour is obtained by an analytic continuation from the imaginary time axis. Since the λ field, considered as a function of imaginary times, satisfies the same boundary condition as the Green's function, it is composed of two analytic pieces which can be continued from imaginary times to complex times on the contour C. Starting from the Fourier transform given by Eq. (8) we obtain, in analogy with Eqs. (20) and (23), the results

$$\lambda^<(\bar{\tau}-\bar{\tau}') = -\frac{1}{\pi}\int_{-\infty}^{\infty} d\omega\, f(\omega) e^{-i\omega(\bar{\tau}-\bar{\tau}')}\, \mathrm{Im}\,\lambda^R(\omega), \quad (32)$$

and

$$\lambda^>(\bar{\tau}-\bar{\tau}') = -\frac{1}{\pi}\int_{-\infty}^{\infty} d\omega[f(\omega)-1] e^{-i\omega(\bar{\tau}-\bar{\tau}')}\, \mathrm{Im}\,\lambda^R(\omega), \quad (33)$$

where $\mathrm{Im}\,\lambda^R(\omega)$ is the spectral function of the λ field. These integrals define analytic functions of imaginary times and can be continued to the contour shown in Fig. 1 simply by substituting $\bar{\tau}\to\bar{t}$ and $\bar{\tau}'\to\bar{t}'$, where $\bar{t}$ and $\bar{t}'$ are on the contour C. Thus, the contour-ordered λ-field can be written as

$$\lambda_c(\bar{t},\bar{t}') = -\frac{1}{\pi}\int_{-\infty}^{\infty} d\omega\, \mathrm{Im}\,\lambda^R(\omega) \times \exp[-i\omega(\bar{t}-\bar{t}')][f(\omega) - \Theta_c(\bar{t}-\bar{t}')], \quad (34)$$

where $\Theta_c=0$ if $\bar{t}$ precedes $\bar{t}'$ on C and $\Theta_c=1$ otherwise, and $\bar{t}$ and $\bar{t}'$ lie anywhere on the contour. Restricting $\bar{t}$ and $\bar{t}'$ to the vertical part of the contour, and using the antiperiodicity along the imaginary axis, we can make the inverse Fourier transform

$$\lambda(i\omega_n) = \lambda_n = i\int_0^{-i\beta} d\bar{\tau}\lambda_c(\bar{\tau},0)e^{-\omega_n\bar{\tau}} = -i\int_0^{-i\beta} d\bar{\tau}\lambda_c(\bar{\tau},-i\beta)e^{-\omega_n\bar{\tau}}, \quad (35)$$

and recover the spectral formula

$$\lambda(i\omega_n) = -\frac{1}{\pi}\int_{-\infty}^{\infty} d\omega \frac{\mathrm{Im}\,\lambda^R(\omega)}{i\omega_n - \omega}. \quad (36)$$

Contrary to the arguments of $G_f(t-t')$, which define the boundaries of the horizontal piece of the contour, the arguments $\bar{t}$ and $\bar{t}'$ of the contour-ordered λ field can be anywhere on the contour C, *so that the dynamical mean field connects the real and the imaginary parts of the contour*. In DMFT, the λ field originates from the electron hopping on the lattice and it is responsible not only for the propagation of particles in real times but for the thermalization of the system as well. Contrary to most nonequilibrium problems, in which the real

field is switched on at some time t_0 and the integration along the vertical part of the Kadanoff-Baym contour can be neglected as one approaches the steady state, in DMFT problems it is essential to integrate over the whole contour, because the hopping on the lattice (which gives rise to the λ field) is always present.

We can now find the contour-ordered Green's function using the Kadanoff-Baym EOM methods, and we consider the case $t > t'$. The fermionic operators on the contour satisfy the EOMs

$$i\frac{d}{d\bar{t}}d^\dagger(\bar{t}) = [\mu - Uf^\dagger(\bar{t})f(\bar{t})]d^\dagger(\bar{t}), \tag{37}$$

and

$$i\frac{d}{d\bar{t}}f(\bar{t}) = [(E_f - \mu) + Ud^\dagger(\bar{t})d(\bar{t})]f(\bar{t}). \tag{38}$$

Since $f^\dagger(\bar{t})f(\bar{t}) = f^\dagger(0)f(0)$ does not change with time (i.e., it commutes with the Hamiltonian), Eq. (37) has a simple solution

$$d^\dagger(\bar{t}) = e^{-i[\mu - Uf^\dagger(t')f(t')](\bar{t}-\bar{t'})}d^\dagger(t'), \tag{39}$$

where t' is the initial time on the contour. The evolution of f electrons is more complicated, because the number of d electrons fluctuates in time and we can only write the solution as a contour-ordered product

$$f(\bar{t}) = e^{-i(E_f-\mu)(\bar{t}-\bar{t'})}S_c'(\chi_t)f(t'), \tag{40}$$

where

$$S_c'(\chi_t) = T_c \exp\left\{\int_c d\bar{\bar{t}}\int_c d\bar{\bar{t}}'\chi_t(\bar{\bar{t}},\bar{\bar{t}}')d^\dagger(\bar{\bar{t}})d(\bar{\bar{t}}')\right\}, \tag{41}$$

and

$$\chi_t(\bar{\bar{t}},\bar{\bar{t}}') = -iU\Theta_c(\bar{t}-\bar{\bar{t}})\delta_c(\bar{\bar{t}}-\bar{\bar{t}}'). \tag{42}$$

Thus, we obtain

$$G_f^>(t-t') = -\frac{e^{-i(E_f-\mu)(t-t')}}{\mathcal{Z}_{at}}\mathrm{Tr}_{df}[e^{-\beta\mathcal{H}_{at}}S_c(\tilde{\lambda}_c)f(t')f^\dagger(t')], \tag{43}$$

where $S_c(\tilde{\lambda}_c)$ is the evolution operator in the presence of the modified time-dependent potential which is due to the fluctuation in the number of d electrons during the propagation of an f electron from the initial time t' to the final time t

$$\tilde{\lambda}_c(\bar{\bar{t}},\bar{\bar{t}}') = \lambda_c(\bar{\bar{t}},\bar{\bar{t}}') + \chi_t(\bar{\bar{t}},\bar{\bar{t}}'). \tag{44}$$

Note, the operator sequence $f(t')f^\dagger(t')$ commutes with $S_c(\tilde{\lambda}_c)$ and removes all the occupied f states from the trace, so that the f propagator can be expressed in terms of a partition function of an effective d electron

$$G_f^>(t-t') = -\frac{e^{-i(E_f-\mu)(t-t')}}{\mathcal{Z}_{at}}\mathcal{Z}(\mu,\tilde{\lambda}_c), \tag{45}$$

where $\mathcal{H}_0$ defines the dynamics of a d electron when there are no f electrons, and

$$\mathcal{Z}(\tilde{\lambda}_c) = \mathrm{Tr}_d[e^{-\beta\mathcal{H}_0}S_c(\tilde{\lambda}_c)] \tag{46}$$

is the partition function of such an electron subject to the effective $\tilde{\lambda}_c$ field. Because of time-translation invariance, we set $t'=0$ from now on.

To find the partition function of a d electron driven by the time-dependent $\tilde{\lambda}_c$ field, we use again functional derivative techniques to define an auxiliary Green's function

$$g^c(\bar{t},\bar{t'}) = \frac{1}{\mathcal{Z}(\tilde{\lambda})}\frac{\delta\mathcal{Z}(\tilde{\lambda}_c)}{\delta\tilde{\lambda}(\bar{t'},\bar{t})}, \tag{47}$$

such that

$$g^c(\bar{t},\bar{t'}) = -\frac{1}{\mathcal{Z}(\tilde{\lambda})}\mathrm{Tr}_d[T_c e^{-\beta H_0}d(\bar{t})d^\dagger(\bar{t'})S_c(\tilde{\lambda}_c)]. \tag{48}$$

Note, the operator dynamics on the contour is now defined by $\mathcal{H}_0$

$$O(\bar{t}) = e^{i(\bar{t}-\bar{t'})\mathcal{H}_0}O(\bar{t'})e^{-i(\bar{t}-\bar{t'})\mathcal{H}_0}. \tag{49}$$

Next, we introduce an auxiliary contour-ordered Green's function for a d electron driven by the χ_t field in the absence of the λ_c field

$$g_0^c(\bar{t},\bar{t'}) = \frac{\delta \ln \mathcal{Z}_0(\chi_t)}{\delta\chi_t(\bar{t'},\bar{t})}, \tag{50}$$

where

$$\mathcal{Z}_0(\chi_t) = \mathrm{Tr}_d[T_c e^{-\beta H_0}S_c(\chi_t)] = 1 + e^{\beta\mu - iUt}, \tag{51}$$

is the effective partition function of such a system. Functional differentiation gives

$$g_0^c(\bar{t},\bar{t'}) = -\frac{1}{\mathcal{Z}_0(\chi_t)}\mathrm{Tr}_d[T_c e^{-\beta H_0}d(\bar{t})d^\dagger(\bar{t'})S_c(\chi_t)]. \tag{52}$$

The evaluation of $\mathcal{Z}_0(\chi_t)$ and g_0^c is straightforward (for details see Refs. 11 and 7), $S_c(\chi_t)$ does not change the number of d electrons and the Hilbert space for the d states comprises only two states ($n_d=0$ and $n_d=1$). The Green's functions g and g_0 depend explicitly on the contour times $\bar{t}$ and $\bar{t'}$, and implicitly on the external time t (recall we set $t'=0$).

Taking the time derivatives of $g^c(\bar{t},\bar{t'})$ and $g_0^c(\bar{t},\bar{t'})$ with respect to $\bar{t}$, we find, using Eq. (49), the EOMs

$$\int_c d\bar{t'}[g^c]^{-1}(\bar{t},\bar{t'})g^c(\bar{t'},\bar{t}) = \delta_c(\bar{t}-\bar{t'}), \tag{53}$$

where

$$[g^c]^{-1}(\bar{t},\bar{t'}) = [g_0^c]^{-1}(\bar{t},\bar{t'}) + \lambda_c(\bar{t},\bar{t'}), \tag{54}$$

and

$$[g_0^c]^{-1}(\overline{t,t'}) = \left(-\frac{\partial}{\partial \overline{t}} + i\mu \right) \delta_c(\overline{t}-\overline{t'}) + \chi_t(\overline{t,t'}). \quad (55)$$

In operator form, this can be written as

$$[g^c]^{-1} g^c = \mathbf{1}, \quad (56)$$

where the unit operator **1** has the matrix elements $\delta_c(\overline{t}-\overline{t'})$. The Dyson equation for the integral operator g^c can thus be written as

$$[g^c]^{-1} = [g_0^c]^{-1}[1 + g_0^c \lambda_c], \quad (57)$$

with the operator product implying an integration over the contour C. From the definition of g_c in terms of the functional derivatives of the partition function $\mathcal{Z}(\tilde{\lambda}_c)$, it follows that

$$\mathcal{Z}(\tilde{\lambda}_c) = e^{\mathrm{Tr}\ \ln[g^c]^{-1}}, \quad (58)$$

where the continuous trace of a contour-ordered operator is given by the line integral over the contour C. Using Dyson's equation, this can be written as

$$\mathcal{Z}(\tilde{\lambda}_c) = \mathcal{Z}_0(\chi_t) e^{\mathrm{Tr}\ \ln(1+g_0^c \lambda_c)}. \quad (59)$$

To approximate the continuous trace by a discrete one,[8] we expand the logarithm

$$\ln(1 + g_0^c \lambda_c) = \sum_{n=1}^{\infty} \frac{1}{n} (g_0^c \lambda_c)^n, \quad (60)$$

and replace each contour integral by a discrete sum, using a discrete quadrature rule

$$\int_c dt\, I(t) = \sum_{i=1}^{N} W_i I(t_i), \quad (61)$$

with weights W_i for the discrete set of times $\{t_1, \ldots, t_N\}$ on the contour C. Then, the multiple integrals in Eq. (60) reduce to matrix multiplication, and we can use the usual expression from linear algebra

$$\mathrm{Tr}\ \ln(1 + g_0^c \lambda_c) = \ln \det(1 + g_0^c \lambda_c), \quad (62)$$

where det represents an $N \times N$ matrix determinant. We obtain the final result

$$G_f^>(t) = -\frac{1}{\mathcal{Z}} e^{-i(E_f-\mu)t} \mathcal{Z}_0(\chi_t) \times \det\left[W_i \left\{ \frac{\delta_{ij}}{\Delta t_c} + \sum_k g^c(t_i,t_k) W_k \lambda_c(t_k,t_j) \right\} \right], \quad (63)$$

which we calculate numerically ($1/\Delta t_c$ is the approximation to the delta function on the contour C with Δt_c the width of the interval that includes the delta function; for a [midpoint] rectangular quadrature rule, one takes $W_i = \Delta t_c$).

III. COMPUTATIONAL RESULTS

The numerical evaluation of the f-electron Green's function appears to be a rather straightforward procedure: one decides on a step size for the real-time axis Δt_{real} and for the imaginary-time axis Δt_{imag} of the Kadanoff-Baym contour and then calculates out to the largest time that is feasible within the limitations of the computational resources. In the results presented here, we take Δt_{real} to range from 0.1 to 0.0125. We fix $\Delta t_{\mathrm{imag}} = 0.05$. The cutoff in time is always taken to be no larger than 80. In order to calculate the f-electron Green's function, we need to calculate the determinant of a discretized matrix operator. This is done by first diagonalizing the matrix, and then taking the product of all of the eigenvalues. This step is the most time-consuming step of the calculation, because the matrix is a general complex matrix, with no special symmetries, and the eigenvalues are usually complex-valued (the maximal matrix size that we consider is about 2100×2100). Since each time t chosen to evaluate the Green's function requires a new contour, the grid of points on the time axis, where $G_f^>(t)$ is generated, need not use the same spacing as the discretizing grid of each Kadanoff-Baym contour used for discretizing the continuous matrix operator. Usually, we use a time-grid spacing of 0.2 or 0.1, because the Green's function does not normally have oscillations that are on a finer scale than that on the time axis. Once the Green's function has been calculated on the time-axis grid, we perform a Fourier transform to calculate it on the real-frequency axis. We first spline our real-time data (using a shape-preserving Akuba spline) onto a real-time grid that is 20 times smaller than the originally chosen time-grid spacing. Next, we numerically sum the (cosine) Fourier transform of the real part of the Green's function to determine the spectral function (which is possible only at half-filling; for other fillings the analysis is more complicated[7]). More details of the numerics can be found elsewhere.[10]

The spectral function satisfies a number of important properties. Since our calculation is an equilibrium calculation (even though we are employing a non-equilibrium formalism), the spectral function is non-negative and the integral of the spectral function over all frequency is equal to 1. Furthermore, the Green's function on the real-time axis approaches $w_1 - 1$ as $t \to 0$ and has an exponentially decaying (and possibly oscillating) behavior at large times. It also increases quadratically in t for small times with a curvature that is independent of temperature. Unlike the conduction density of states (DOS), which is independent[12] of temperature, the f-electron DOS evolves[8] with T. But, because the value at $t=0$ [and the first and second derivative of Re $G_f^>(t)$] is the same for all temperatures, we find that the deviations of the real-time Green's functions (due to changes in the temperature) increase at large times.

When the DOS develops a gap at low temperature, the long-time behavior of the Green's function develops significant oscillations, with an amplitude that can decay to zero very slowly. This creates numerical problems, since it implies that the cutoff in time needs to be large in order to be able to accurately determine the DOS. Indeed, we will find that this cutoff dependence limits our ability to accurately determine the DOS at low temperature.

We begin our discussion with a plot of the real part of the (greater) Green's function versus time for $T=1$ on the Bethe lattice and for five different values of U (Fig. 2); recall our units are $t^*=1$. The values of Δt_{real} are 0.0125 for

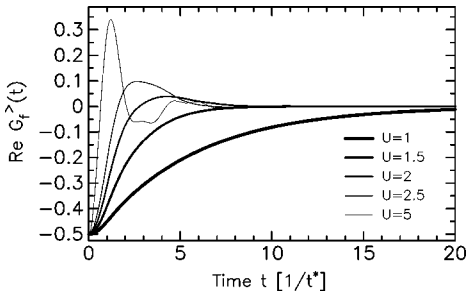

FIG. 2. Real part of the (greater) *f*-electron Green's function as a function of time for $T=1$ and five different values of U on the Bethe lattice.

$U=1, 0.025$ for $U=2$, and $U=5$ and 0.05 for $U=2$ and $U=2.5$. Notice how the Green's function appears to have just a smooth exponential decay for small U, but as U increases, we first see the Green's function assume positive values, and then we see that it picks up significant oscillations, whose period decreases as U increases. When U is small enough that there is no gap in the DOS, then we find that the long-time behavior is exponentially decaying (with oscillations entering as the critical value of U for the Mott transition is approached). In this regime, we can extrapolate the results for small time out to large time, by fitting the Green's function tail with an exponential function, and evaluating that function out to long times. This allows us to use a smaller time cutoff (and thereby a smaller Δt_{real}), which becomes increasingly important at low temperature in order to maintain high quality in the data.

In Fig. 3, we plot the logarithm of the absolute value of the real part of the (greater) Green's function for $T=0.2$ and $U=1.5$ on the Bethe lattice. Note how the tails of the Green's functions show perfect exponential decay at large time. The exponent depends strongly on the discretization Δt_{real} of the Kadanoff-Baym contour. But, because of this simple exponential behavior, we can append extrapolated tails to our more accurate calculations (with smaller Δt_{real}) and construct good Fourier transforms. Unfortunately, there does not seem to be any simple way to extrapolate the results to the limit $\Delta t_{\text{real}} \to 0$ on the time axis. The problem is that the systematic error due to a finite Δt_{real} is not arising from a Trotter breakup which has a simple error term, but rather is arising from the discretization of the continuous matrix operator.

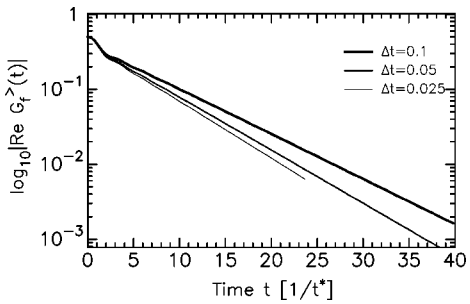

FIG. 3. Logarithm of the absolute value of the real part of the (greater) *f*-electron Green's function as a function of time for $T=0.2$ and $U=1.5$ on the Bethe lattice. Three different values of Δt_{real} are shown.

When U is large enough that the tails of the Green's functions show oscillatory behavior on top of the decaying behavior, we have no simple way to extrapolate the tails out to large time, and the errors of the calculations become larger. [One might have wanted to extrapolate $\ln|G_f^>(t)|$ on the time axis to $\Delta t \to 0$, but that cannot be done once $G_f^>(t)$ crosses zero.]

When we perform the cosine Fourier transform of the real part of $G_f^>(t)$ to get the *f*-electron spectral function, we first spline the real-time data (with an exponentially decaying tail appended if appropriate) onto a grid that is 20 times finer using a shape-preserving Akuba spline, and then numerically perform the Fourier transform. Next, we try to extrapolate the Fourier transform to $\Delta t_{\text{real}} \to 0$. This extrapolation is performed using an *n*-point Lagrange interpolation formula (pointwise in ω) on the different DOS generated for the different Δt_{real}. Such a procedure allows for higher order polynomial approximations to the extrapolation as more data are included. We sometimes find that, even though we have data for a number of different Δt_{real} values, it is most accurate to perform a linear extrapolation for the two smallest values of Δt_{real}. We call this extrapolation scheme δ extrapolation.

We judge the accuracy of our calculations in a number of different ways. The first thing we do is to compare the moments of the DOS [with or without an extra factor of $f(\omega)$] to exact results for those moments (see below). We also compare the Matsubara frequency Green's functions (generated from an independent program that works directly on the imaginary axis[7,8,11]) with the Matsubara frequency Green's function generated by integrating the spectral formula (with the given DOS) for each Matsubara frequency

$$G_f(i\omega_n) = \int d\omega\, A_f(\omega) \frac{1}{i\omega_n - \omega}. \tag{64}$$

One of the important checks of our numerical accuracy comes from a careful comparison of the calculated results with a number of different moment sum rules of the DOS. The sum rules can be derived in a straightforward fashion: the DOS is first expressed as the imaginary part of the Fourier transform of the real-time retarded Green's function. By introducing complete sets of states, the time dependence of the operators can be expressed in terms of the many-body energies of the different states (note that because this calculation is performed for the impurity, one must include the evolution operator of the λ field, but since it commutes with the *f*-electron operators, it provides no further complications). These can then be integrated over time, and when the imaginary part is taken, one gets a delta function in frequency, which allows the frequency integral to be performed. Finally, any energy factors that remain can be replaced by the Hamiltonian, and the sums over the complete sets of states can be performed. In the end, we are left with operator averages to evaluate. These results are summarized in Table I. Note that when we perform actual calculations, we always add a small shift to the DOS in order to satisfy the zero moment sum rule to at least one part in 10^5 (typically this means adding a shift no larger than 0.005 to the spectral function).

TABLE I. Sum rules for the f-electron DOS. The expectation value $\langle\mathcal{O}\rangle$ denotes $\mathrm{Tr}[e^{-\beta\mathcal{H}_{at}}S(-i\beta,\lambda)\mathcal{O}]/\mathcal{Z}_{at}$. The column on the far right gives the results for the half-filled case considered here. The symbol χ_{mixed} denotes the mixed static local charge susceptibility between the conduction and the localized electrons. Recall at half-filling $E_f=0$, $\mu=U/2$, $w_1=1/2$, and $\rho_e=1/2$.

Moment	Operator average	General result	Half-filling result
$\int d\omega A_f(\omega)$	$\langle\{f,f^\dagger\}_+\rangle$	1	1
$\int d\omega A_f(\omega)f(\omega)$	$\langle f^\dagger f\rangle$	w_1	1/2
$\int d\omega A_f(\omega)\omega$	$-\langle[\mathcal{H},f]f^\dagger\rangle+\langle[\mathcal{H},f^\dagger]f\rangle$	$E_f-\mu+U\rho_e$	0
$\int d\omega A_f(\omega)\omega f(\omega)$	$\langle[\mathcal{H},f^\dagger]f\rangle$	$(E_f-\mu)w_1+U(\chi_{\mathrm{mixed}}+w_1\rho_e)$	$U\chi_{\mathrm{mixed}}$
$\int d\omega A_f(\omega)\omega^2$	$\langle[\mathcal{H},[\mathcal{H},f]]f^\dagger\rangle+\langle[\mathcal{H},[\mathcal{H},f^\dagger]]f\rangle$	$(E_f-\mu)^2+(2E_f-2\mu+U)U\rho_e$	$U^2/4$
$\int d\omega A_f(\omega)\omega^2 f(\omega)$	$\langle[\mathcal{H},[\mathcal{H},f^\dagger]]f\rangle$	$(E_f-\mu)^2w_1+(2E_f-2\mu+U)U(\chi_{\mathrm{mixed}}+w_1\rho_e)$	$U^2/8$

We find that sometimes the δ-extrapolation scheme does not further improve the accuracy of the spectral function. In that case, it is often more accurate to use the result generated with the smallest Δt_{real}. In other cases, we find that the exact result for the lowest Matsubara frequency Green's function is bracketed by the calculation with the smallest Δt_{real} and the δ-extrapolation result. In that case, we can average those two spectral functions in order to produce better agreement for $G_f(i\omega_0)$. We call this extrapolation procedure Matsubara extrapolation. It sometimes can improve the accuracy of the results.

As a general rule of thumb, if we can achieve accuracy of better than 1% for all of the spectral moments, and we can achieve four digits of accuracy for all of the Matsubara frequency Green's functions, then the resulting DOS is numerically quite accurate. The deviations from the exact result are most likely occurring at small frequencies, where we need long-time data to get an accurate Fourier transform, and at high frequencies, where the tails don't always decay exactly to zero.

We illustrate these extrapolation procedures with the case $U=1.5$ on the Bethe lattice (results for $U=1$ have also appeared[10]). We first focus on high temperature, with $T=5$. The results for the moment sum rules, for the shift to the DOS, and for the lowest Matsubara frequency Green's function are presented in Table II. We plot the DOS for different Δt_{real} in Fig. 4. As can be seen in the figure, as the discretization size decreases, the DOS approaches a limiting result, which is close to the one predicted by the δ-extrapolation procedure. An examination of the table shows how the moment sum rules and the Matsubara frequency Green's functions are all improved as the discretization error is reduced. The extrapolation formula used a quadratic Lagrange interpolation with all the three DOS calculated at different Δt_{real}'s. These results show that a systematic extrapolation procedure is sometimes possible, and that the overall accuracy that can be achieved is quite high (of course it is difficult to estimate the pointwise accuracy of the DOS from any of these integral sum rules).

As the temperature is lowered, the spectral function sharpens when U is small. In the noninteracting case, the spectral function is a delta function. In the interacting case, the spectral function approaches a delta function, but always maintains a finite width, even at $T=0$. Nevertheless, the calculations become more difficult at lower T, because a narrow peak in the DOS implies a slow exponential decay in $G_f^>(t)$, and we find that the discretization error also grows as T is reduced. To illustrate this phenomenon we show results for $U=1.5$ and $T=0.1$. The moment sum rules are summarized in Table III and the DOS are summarized in Fig. 5. One can see that as Δt_{real} is made smaller, the peak in the DOS is reduced in height and increases in width. Furthermore, the δ-extrapolation scheme seems to overcorrect, by producing a DOS that is too wide (we use a two-point [linear] interpolation formula here). The Matsubara-extrapolation procedure is much better, but the overall accuracy is reduced relative to

TABLE II. Table of the accuracy of the different calculations of the DOS by comparing results for the different sum rules ($U=1.5$ on the Bethe lattice, with $T=5$). The frequency cutoff for the zero moment sum rule is $|\omega|<15$, while all other moments are cut off at the point where the integral stops increasing and approaches a constant (there is usually a decrease for larger values of ω) which normally corresponds to $|\omega|<4$.

Moment	$\Delta t_{\mathrm{real}}=0.1$	$\Delta t_{\mathrm{real}}=0.05$	$\Delta t_{\mathrm{real}}=0.025$	δ extrapolation	Exact
1	0.999994217	1.00000354	1.0000113	1.00000099	1
$f(\omega)$	0.502728929	0.501524381	0.500528293	0.49994769	0.5
$\omega f(\omega)$	−0.023149398	−0.025185717	−0.026169934	−0.02785382	−0.027912
ω^2	0.465833709	0.507191087	0.527187957	0.56173037	0.5625
$\omega^2 f(\omega)$	0.232916854	0.253595543	0.263593979	0.28086519	0.28125
$G_f(i\omega_0)$	−0.063584452	−0.063571673	−0.063545431	−0.06351812	−0.063518334
Shift	0.00485	0.005015	0.002534	−0.0000039	0

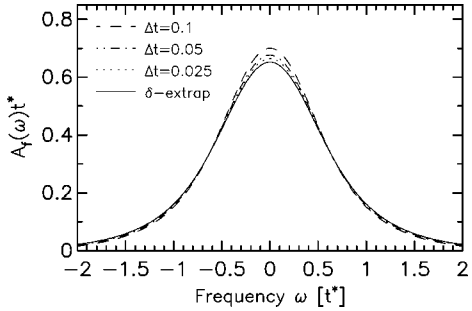

FIG. 4. *f*-electron DOS for different discretization sizes. Also plotted is the δ-extrapolated result using a three-point (quadratic) Lagrange interpolation formula. The parameters are $U=1.5$ on the Bethe lattice, with $T=5.0$.

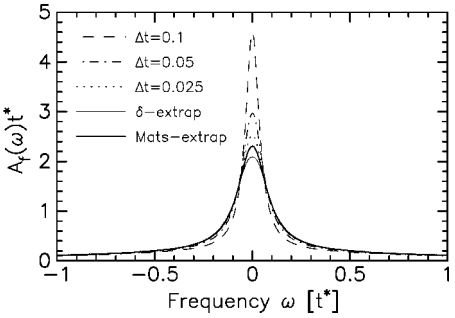

FIG. 5. *f*-electron DOS for different discretization sizes. Also plotted is the δ-extrapolated result using a linear interpolation formula for the smallest two Δt_{real} values and the Matsubara extrapolated result. The parameters are $U=1.5$ on the Bethe lattice, with $T=0.1$.

the higher temperature results (we find only about 3% accuracy for the moments, and three parts in 10^3 accuracy for the Matsubara frequency Green's functions). We find that this behavior is generic for our calculations—usually the calculations are more difficult at lower temperature, often requiring a smaller discretization size for the same level of accuracy. We also find that the real-frequency extrapolation procedures start to break down as T is reduced too.

A summary of the results for the case of $U=1.5$ on the Bethe lattice is shown in Fig. 6. We have used the most accurate DOS calculated at each temperature, by one of the two extrapolation procedures. We also included the conduction electron DOS, which has a dip develop at the Fermi energy. One can see that the *f*-electron DOS grows and sharpens as T is reduced. We find that calculations at much lower temperatures than presented here become problematic due to discretization and time-domain cutoff errors. Inset into the figure is a plot of $1/A_f(\omega=0)$ versus T. We have linearly extrapolated the last few points to estimate how big the DOS would grow as $T\rightarrow 0$. Our estimate shows that the peak in the DOS should increase to about 4.5 as $T\rightarrow 0$. Note the major differences between the localized electron DOS and the conduction electron DOS. The *f*-electron DOS sharpens and concentrates much weight around $\omega=0$, while the conduction electron DOS has a dip there. Notice further that there is no significant change that we can see in our data near the band edge of the conduction electron DOS that is also seen in the *f*-electron DOS, although we expect that at $T=0$ the bandwidths of both DOS should agree with each other.

We next investigate the case $U=2.5$ on the Bethe lattice (results for the critical interaction strength $U=2$ appear elsewhere[9]). This case corresponds to lying just on the insulating side of the metal-insulator transition (which occurs at $U=2$). The summary plot of the DOS is presented in Fig. 7. Note how the localized electron DOS sharpens and develops a gap as T is lowered. What is interesting is that the DOS seems to pile up near the correlation-induced gap at low T. We also see a kink start to develop near the upper and lower conduction band edges, indicating that the *f*-electron DOS will likely vanish outside of the band as $T\rightarrow 0$. Numerically, these calculations are challenging. If the discretization error is too large, or the time-domain cutoff is too small, then we can find negative DOS in the gap region at low temperature. In fact, the poor quality of our data for larger Δt_{real} is the reason why we cannot extrapolate the low-temperature data faithfully. The accuracy of our calculations is usually better than 1.5% for the first moment, better than 4% for the second moment, and better than 0.5% for the Matsubara frequency

TABLE III. Table of the accuracy of the different calculations of the DOS by comparing results for the different sum rules ($U=1.5$ on the Bethe lattice, with $T=0.1$). The frequency cutoff for the zero moment sum rule is $|\omega|<15$, while all other moments are cutoff at the point where the integral stops increasing and approaches a constant (there is usually a decrease for larger values of ω) which normally corresponds to $|\omega|<4$.

Moment	$\Delta t_{\text{real}}=0.1$	$\Delta t_{\text{real}}=0.05$	$\Delta t_{\text{real}}=0.025$	δ extrapolation	Mats-extrapolation	Exact
1	1.00015473	1.00000776	1.00000629	0.99999920	1.0000015	1
$f(\omega)$	0.503123093	0.501181165	0.500012329	0.50005666	0.5003576	0.5
$\omega f(\omega)$	−0.192872666	−0.208532743	−0.215836651	−0.22736437	−0.2227881	−0.220742
ω^2	0.477461453	0.518025518	0.537836969	0.58728661	0.5699565	0.5625
$\omega^2 f(\omega)$	0.238730727	0.259012759	0.268918484	0.29364330	0.2849782	0.28125
$G_f(i\omega_0)$	−2.08188686	−1.96833103	−1.91591427	−1.86349693	−1.8890850	−1.88908508
$G_f(i\omega_1)$	−0.882512945	−0.865141592	0.85643369	−0.847725223	−0.851976249	−0.854845179
Shift	0.00501	0.005060	0.002544	−0.0000091	−0.0004000	0

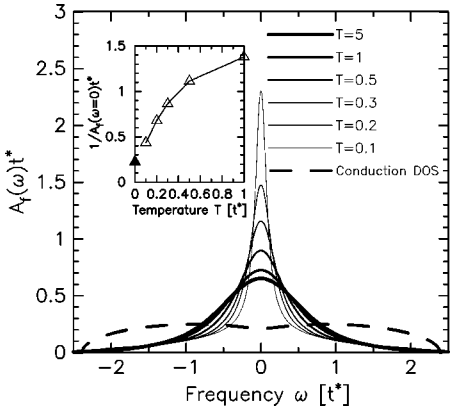

FIG. 6. *f*-electron DOS for different temperatures. Also plotted is the conduction-electron DOS (which is temperature independent). The parameters are $U=1.5$ on the Bethe lattice. Inset is a plot of $1/A_f(\omega=0)$ versus T. Note how it appears to behave linearly at small T, allowing us to extrapolate to the $T=0$ result, so we can predict the maximal height of the *f*-electron DOS at $T=0$.

Green's functions (at higher temperature, we do significantly better).

We have also performed calculations for a large-gap insulator on the Bethe lattice, with $U=5$. The summary plot is shown in Ref. 10. The results show a conduction-electron DOS with a large gap of about $2.5t^*$. At high temperature, the *f*-electron DOS has significant subgap states. As T is lowered, we find a transfer of spectral weight out of the gap region, with the weight in the peaks moving towards the gap, and then some additional weight being transferred to shoulders that lie close to the conduction band edges. There are small oscillations in the gap region for $T=0.8$ that are artifacts of the cutoff in time. In these calculations, we do not perform any extrapolations; instead, we use the smallest Δt_{real} that produces a positive DOS everywhere, and does not develop significant oscillations due to the finite time cutoff. These values are the following: for $T=5$ and $T=2$ we use $\Delta t_{\text{real}}=0.05$; for $T=1$ and $T=0.8$ we use $\Delta t_{\text{real}}=0.025$. When we compare the *f*-electron DOS to the conduction-electron DOS, we find that the conduction electron DOS has more spectral weight at higher frequency up to the band edge—the *f*-electron DOS spills out beyond the conduction band edge for finite T, but this weight is reduced as T is lowered. It is difficult to go to lower temperatures, as computer resources are rapidly exhausted.

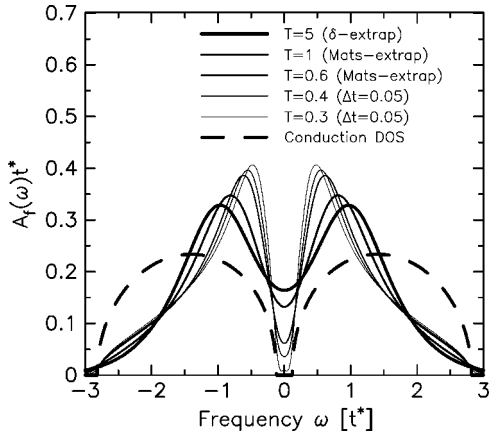

FIG. 7. *f*-electron DOS for different temperatures with $U=2.5$ on the Bethe lattice. Also plotted is the conduction-electron DOS (which is temperature independent). The $T=5$ data uses δ extrapolation, the $T=1$ and 0.6 data use the Matsubara-extrapolation procedure, and the lower temperatures are not extrapolated (but have $\Delta t_{\text{real}}=0.05$). Note how the *f*-electron DOS develops a gap as T is lowered. Note further that a kink starts to develop near the upper and lower band edges of the conduction DOS as expected too. Our computational accuracy is worst for the subgap DOS at low temperature.

We also present results for the hypercubic lattice. The hypercubic lattice does not develop gaps at the metal-insulator transition due to the infinite exponential tails of the noninteracting Gaussian DOS. But, the spectral function is suppressed to zero at the Fermi energy and there is a "gap region" where the DOS remains exponentially small. The transition occurs at $U=\sqrt{2}$, and we expect results for the hypercubic lattice to be similar to those of the Bethe lattice when $U_{\text{Bethe}}=\sqrt{2}U_{\text{hypercubic}}$. Brandt and Urbanek's original work[8] presented results for the hypercubic lattice. Unfortunately they gave no details on the step sizes used in their computations or of the accuracy of their results. The one discussion of moments that they include gives an improper value to the second moment of the *f*-electron DOS, and it is likely they never checked the numerical accuracy of their results against any moment sum rules.

We calculate three different values of U for the hypercubic lattice: $U=1$, which has a dip in the conduction electron DOS (similar to $U=1.5$ for the Bethe lattice); $U=2$, which is a "small-gap" insulator (similar to $U=2.5$ on the Bethe lattice); and $U=4$, a "large-gap" insulator (similar to $U=5$ on the Bethe lattice); the near-critical point $U=1.5$ appears elsewhere.[9] Brandt and Urbanek showed two DOS for $U=1$ and five DOS for $U=2$. They did not calculate the $U=4$ case.

The $U=1$ case is plotted in Fig. 8. The results shown here are quite similar to those on the Bethe lattice (Fig. 6). The DOS sharpens as T is lowered, even though the conduction-electron DOS has a dip at the Fermi energy. Inset is a plot of the inverse of the DOS at the chemical potential versus T. We can use it to extrapolate to $T=0$ and predict that the spectral function peaks at about 4.5. Our results at high temperature and at low temperature agree well with those of Brandt and Urbanek.[8]

Next, we consider the case $U=2$ in Fig. 9, which should be compared to the similar results on the Bethe lattice (Fig. 7). Here, we see the same kind of behavior—the gap is filled at high temperature; as T is lowered, spectral weight transfers from the gap region out to the band edges, and the peaks of the DOS migrate toward the gap regions. Note that the data shown for $T=0.2$ actually have a small region of frequency where the DOS becomes negative. This is an artifact of the discretization error and the time-domain cutoff.

The results for $U=4$ on the hypercubic lattice are presented in Fig. 10. The behavior is what one expects: at high temperature, the gap region is filled in by thermal excitations. As the temperature is lowered, the gap region develops, with spectral weight being transferred from the gap out

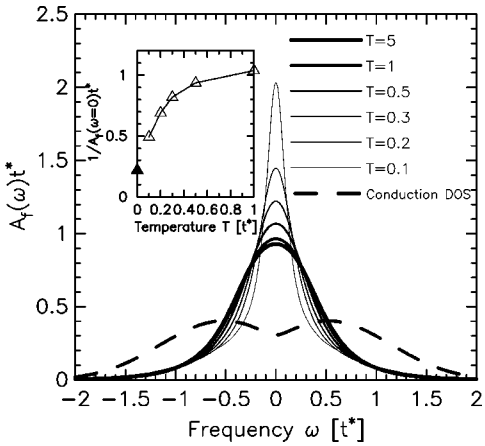

FIG. 8. *f*-electron DOS for different temperatures with $U=1$ on the hypercubic lattice. Also plotted is the conduction-electron DOS. All of the data were extrapolated with one of the two extrapolation techniques discussed in the text. Note the similarity with Fig. 6 for the Bethe lattice. In the inset we plot the inverse of the DOS at the chemical potential. Here, the low-temperature results don't appear to behave in quite the linear fashion we saw on the Bethe lattice, but we can still attempt to extrapolate to $T=0$ with the prediction that the peak in the DOS will also be around 4.5 at $T=0$.

to higher energy. As the temperature becomes even lower, the computational needs exceed our resources. Note how the peaks in the *f*-electron DOS are pushed closer to the gap region than the peaks in the conduction-electron DOS.

IV. CONCLUSIONS

In this contribution we calculated the *f*-electron DOS of the Falicov-Kimball model at half-filling. The procedure requires us to generate the greater Green's function for real time and the Fourier transform to get the DOS. Unlike the conduction DOS, which is temperature independent, the

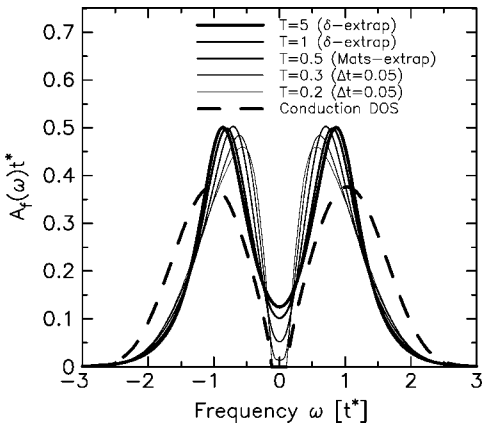

FIG. 9. *f*-electron DOS for different temperatures with $U=2$ on the hypercubic lattice. Also plotted is the conduction-electron DOS. The data are either extrapolated with one of the two extrapolation techniques discussed in the text, or we work with a fixed value of the discretization on the real-time axis. Note the similarity with Fig. 7 for the Bethe lattice.

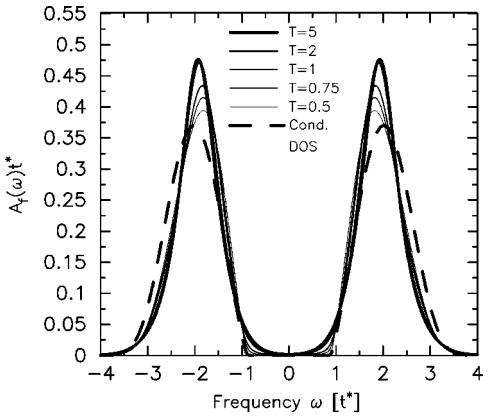

FIG. 10. *f*-electron DOS for different temperatures with $U=4$ on the hypercubic lattice (the $T=5$ and $T=2$ data overlap). Also plotted is the conduction-electron DOS. The $T=5$ data are calculated with the δ-extrapolation technique; all other temperatures work with $\Delta t_{\text{real}}=0.05$. These results are similar to those found for the Bethe lattice (Ref. 10), but for the Bethe lattice the difference between the *f*-electron DOS and the conduction electron DOS is more dramatic.

f-electron DOS has significant temperature dependence. For small U, the DOS sharpens as T is lowered to a single-peak structure with a narrow width. For large U, the DOS develops a gap at low T and the peaks of the DOS push close to the correlation-induced gap edges. When we compare results for similar U values on the Bethe and hypercubic lattices, we see similar behavior in the DOS.

We performed an in-depth analysis of the accuracy of the numerical calculations. Errors arise from a finite discretization error (discretizing the continuous matrix operator into a discrete matrix) and a time-domain cutoff error [representing the largest time t that $G_f^>(t)$ is calculated out to]. We use linear and quadratic moment sum rules and the spectral formula for the Matsubara frequency Green's functions to gauge the accuracy of the calculations. In general, the discretization error becomes worse as $T\rightarrow 0$, and it is quite challenging to get accurate results at low temperatures and strong coupling.

This study is useful to understand problems with the accuracy of truly nonequilibrium calculations that use similar Kadanoff-Baym contours. While we would not have exact sum rules to compare to anymore, it is clear that one needs to perform systematic studies in the discretization size along the contour to gauge the accuracy of the results. One also needs to reduce the real-axis discretization as the temperature is reduced. True nonequilibrium problems evolve in an external field, and such a field can be added into the analysis given here. The complicated aspect is being able to construct the local Green's function from the local self-energy, as the coupling to a vector potential enters into the hopping part of the Hamiltonian, and the local Green's function is no longer represented by a simple Hilbert transform.

We only examined the half-filled case here. This provides a significant simplification, as the DOS can be calculated by a Fourier transform of the real part of $G_f^>(t)$. For other fillings, the analysis is more complicated and usually requires using the particle-hole transformation (for calculations with

fillings ρ_e and w_1 and with fillings $1-\rho_e$ and $1-w_1$) to generate the full DOS. This is because the exponential factors in $f(\omega)-1$ suppress the spectral function for $\omega<0$, so only $\omega>0$ results can be determined accurately; by using the particle-hole transformation for the conjugate fillings, we can construct the full DOS. We plan to examine that case in the future.

Note added in proof: After completing this manuscript, we were informed of similar work by F. B. Anders and G. Czycholl (cond-mat/0411721) which efficiently solves for the *f*-electron spectral function using the complimentary approach of the numerical renormalization group. Their work is most accurate at low frequencies and shows the development of x-ray edge singularities in the metallic phase as $T\rightarrow 0$.

ACKNOWLEDGMENT

We acknowledge support from the National Science Foundation under Grant No. DMR-0210717 and the Office of Naval Research under Grant No. N00014-99-1-0328. Supercomputer time was provided by the ERDC and ARSC supercomputer centers.

*Electronic address: freericks@physics.georgetown.edu
†Electronic address: turk@physics.georgetown.edu
‡Electronic address: zlatic@ifs.hr

[1] L. P. Kadanoff and G. Baym, *Quantum Statistical Mechanics* (Benjamin, New York, 1962).
[2] L. V. Keldysh, Zh. Eksp. Teor. Fiz. **47**, 1945 (1964) [Zh. Eksp. Teor. Fiz. **20**, 1018 (1965)].
[3] L. M. Falicov and J. C. Kimball, Phys. Rev. Lett. **22**, 997 (1969).
[4] W. Metzner and D. Vollhardt, Phys. Rev. Lett. **62**, 324 (1989).
[5] U. Brandt and C. Mielsch, Z. Phys. B: Condens. Matter **75**, 365 (1989).
[6] G. Czycholl, Phys. Rev. B **59**, 2642 (1999).
[7] J. K. Freericks and V. Zlatić, Rev. Mod. Phys. **75**, 1333 (2003).
[8] U. Brandt and M. P. Urbanek, Z. Phys. B: Condens. Matter **89**, 297 (1992).
[9] J. K. Freericks, V. M. Turkowski, and V. Zlatić, Physica B (to be published).
[10] J. K. Freericks, V. M. Turkowski, and V. Zlatić, *Proceedings of the 2004 Users Group Conference* (IEEE Computer Society, Los Alamitos, CA, 2005), p. 7.
[11] V. Zlatić, J. K. Freericks, R. Lemański, and G. Czycholl, Philos. Mag. B **81**, 1443 (2001).
[12] P. G. J. van Dongen, Phys. Rev. B **45**, 2267 (1992).